Springer

KSME

Journal of Mechanical Science and Technology 25 (9) (2011) 2195~2209
www.springerlink.com/content/1738-494x
DOI 10.1007/s12206-011-0610-x

Free vibration analysis of solar functionally graded plates with temperature-dependent material properties using second order shear deformation theory †

A. Shahrjerdi[1,2,*], F. Mustapha[2], M. Bayat[3] and D. L. A. Majid[2]

[1]*Department of Mechanical Engineering, MalayerUniversity, Malayer, 65719, Iran*
[2]*Department of Aerospace Engineering, Universiti Putra Malaysia, 43400, Selangor, Malaysia*
[3]*Department of Civil Engineering, Aalborg University, 9000 Aalborg, DK*

(Manuscript Received February 26, 2011; Revised May 22, 2011; Accepted June 6, 2011)

Abstract

Second-order shear deformation theory (SSDT) is employed to analyze vibration of temperature-dependent solar functionally graded plates (SFGP's). Power law material properties and linear steady-state thermal loads are assumed to be graded along the thickness. Two different types of SFGP's such as ZrO_2/Ti-6Al-4V and Si_3N_4/SUS304 are considered. Uniform, linear, nonlinear, heat-flux and sinusoidal thermal conditions are imposed at the upper and lower surface for simply supported SFGPs. The energy method is applied to derive equilibrium equations, and solution is based on Fourier series that satisfy the boundary conditions (Navier's method). Non-dimensional results are compared for temperature-dependent and temperature-independent SFGP's and validated with known results in the literature. Numerical results indicate the effect of material composition, plate geometry, and temperature fields on the vibration characteristics and mode shapes. The results obtained using the SSDT are very close to results from other shear deformation theories.

Keywords: FGM; Solar functionally graded plate; Second-order shear deformation; Temperature-dependent properties; Vibration analysis

1. Introduction

In recent years, solar energy has become an increasingly important area in applied engineering. One of the most significant parts of this field is the solar plate. A solar plate is used to focus solar radiation onto an absorber located at the focal point in a parabolic dish concentrator to provide solar energy. A concentrating solar collector consists of a reflector over the solar plate, an absorber and housing. A parabolic disc is made from pieces of solar plates. The performance of a solar plate in terms efficiency, service life and optical alignment depends on the material and operating conditions. Normally, a solar plate can be fabricated from polished pure material or a coated plate with a special coating [1]. However, some specific applications (such as solar satellites, solar power towers and solar power heat engines) demand low weight and high temperature resistance to avoid undesirable deformation [2]. Functionally graded materials (FGMs) are designed to be thermal barrier materials for aerospace structural applications and fusion reactors [3]. Flexible properties and high thermal resistance provides suitable stiffness to avoid unsought deformation to better optical alignment. It has been reported that FG plates have much lower weight and better heat resistance than pure material plate products of similar size. FGMs usually are composed of a ceramic and a metal, where the volume fraction of the two materials is variable [4]. Based on the literature, a considerable amount of work has been reported on the vibration characteristics of isotropic plates and composite laminates [5, 6]. To determine the small and large deflections, static, linear and non-linear dynamic behavior of FG plates, shear deformation theories of the first, second and third order can be effective tools [7].

Finite element methods (FEM) and first-order shear deformation theory (FSDT) were employed by Praveen and Reddy [8] for nonlinear transient thermo-elastic responses of FG plates. Mokhtar et al. [9] investigated thermal buckling analyses of S-FG plates by using FSDT. The thermal buckling was carried out under uniform, linear and sinusoidal temperature rise across the thickness. Shukla and Huang [10] presented nonlinear static and dynamic responses of the temperature-dependent FG rectangular plate using FSDT. Ibrahim et al. [11] used nonlinear FEM model to assess the nonlinear random response of FG panel subject to combined thermal and acoustic loads by applying FSDT and Von-Karman geometric nonlinearity. Park and Kim [12] presented thermal post buckling and vibration behavior of the FG plates based on FSDT.

† This paper was recommended for publication in revised form by Associate Editor Ohseop Song

*Corresponding author. Tel.: +6089466400, Fax.: +60386567125
E-mail address: alishahrjerdi2000@yahoo.com

Initial displacement and initial stress for nonlinear temperature-dependent material properties were adopted in their research. Zhao et al. [13] employed a element-free kp-Ritz method to analyze the free vibration of temperature-dependent FG plates based on FSDT. Ferreira and Batra [14] provided a global collocation method for natural frequencies of FG plates by a meshless method and applying FSDT. Bayat et al. [15] examined small and large deflection of FG rotating disc by applying FSDT and Von Karman theory. Later, Bayat et al. [16] obtained small deflection of an FG rotating disc with constant and variable thickness profile under thermo-mechanical load using FSDT. Batra and Jin [17] used the FSDT with the FEM to study free vibrations of an FG anisotropic rectangular plate with various boundary conditions.

Several studies were conducted on three-dimensional exact solutions, and other shear deformation theories (such as a third-order-shear deformation theory (TSDT)) for FG plates have been considered [18]. To determine the effects of nonlinearity, Huang et al. [19] compared vibration and dynamic response of temperature dependent FG plates in thermal environment based on the higher-order shear deformation theory. Matsunaga [20] conducted the thermal buckling of temperature-independent FG plates according to a 2D higher-order shear deformation theory. Kim [21] demonstrated vibration characteristics of pre-stressed temperature-dependent FG rectangular plates in thermal environment. In his major study, Kim [21], identified two thermal conditions, linear and nonlinear, with the Rayleigh-Ritz method based on TSDT. Sundararajan et al. [22] employed nonlinear formulation based on von Karman's assumptions to study the free vibration characteristics of temperature dependent FG plates subjected to uniform thermal environments. Chen et al. [23] derived nonlinear partial differential equations for the vibration motion of an initially stressed temperature-independent FGP. Yang and Shen [24] found the dynamic response of initially stressed temperature-dependent FG rectangular thin plates based on Reddy's higher-order shear deformation plate theory and included the thermal effects due to uniform temperature variation. They applied the same method [25] to study the dynamic stability and free vibration of FG cylindrical panels subjected to combined loads and uniform thermal environment.

Some studies apply second-order shear deformation theory (SSDT). Khdeir and Reddy [26] studied the free vibration of laminated composite plates using SSDT. A general formulation for FG circular and annular plates presented by Saidi and Sahraee [27] using SSDT and developed the bending solution that accounts for deflections and various boundary conditions. Shahrjerdi et al. [28] presented free vibration analysis of a quadrangle FG plate by using Navier's method based on SSDT, and then used SSDT for stress analysis of FG solar plates subjected to in-plane and out-plane mechanical loads [29]. Bahtuei and Eslami [30] also conducted the coupled thermo-elastic response of an FG circular cylindrical based on SSDT. Thermal loads were not considered in these studies [26, 28-30].

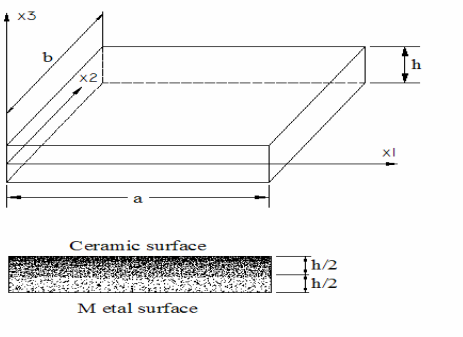

Fig. 1. Solar functionally graded plate.

Many of the above-mentioned papers deal with temperature-independent materials with shear deformation theories. Temperature-dependent materials in a constant temperature field and temperature variations with surface-to-surface heat flow through the thickness direction were considered in other research by applying first, third and higher order shear deformation theories. To the authors' knowledge, few works have been done in the area of dynamic stability of FGM plate by using SSDT. In this paper, the analytical solution is provided for the vibration characteristics of SFGPs under temperature field and applying SSDT. The temperature is assumed to be constant in the plane of the plate. The variation of temperature is assumed to occur in the thickness direction only. The SFGPs are assumed to be simply supported with temperature-dependent and independent material properties with a power-law distribution in terms of the volume fractions of the constituents and subjected to uniform, linear, nonlinear, heat flux and sinusoidal temperature rise. The frequency equation is obtained using Navier's method based on SSDT. This work aims to show the effect of material compositions, plate geometry and temperature fields on the vibration characteristics. Furthermore, the effects of temperature dependency of SFGPs for some types of thermal condition are investigated.

2. Gradation relations

There are some models in the literature that express the variation of material properties in FGMs [9, 16]. The most commonly used is the power law distribution of the volume fraction. Here, an SFGP rectangular in Cartesian coordinate system (x_1, x_2, x_3) with constant thickness h, width a, and length b is considered as shown in Fig. 1. The materials at the top surface ($x_3 = h/2$) and bottom surface ($x_3 = -h/2$) are, respectively, pure ceramic and metal. Between these two pure materials, a power-law distribution of material is applied. According to this model, the material properties of SFGPs are assumed to be position and temperature- dependent and can be expressed as the following [21]:

$$\Gamma = \Gamma\left(x_3, T\right) = \left(\Gamma_c(T) - \Gamma_m(T)\right)\left(x_3/h + 1/2\right)^p + \Gamma_m(T) \qquad (1)$$

Table 1. Temperature-dependent coefficients for ZrO_2/Ti-6Al-4V and Si_3N_4/SUS304.

Material		P_{-1}	P_0	P_1	P_2	P_3
E	SUS304	0	201.04	3.079e-4	-6.534e-7	0
	Si_3N_4	0	348.43	-3.070 e-4	2.160e-7	0
	Ti-6Al-4V	0	122.70	-4.605 e-4	0	0
	ZrO_2	0	132.20	-3.805 e-4	-6.127e-8	0
υ	SUS304	0	0.3262	-2.002 e-4	3.797e-7	0
	Si_3N_4	0	0.2400	0	0	0
	Ti-6Al-4V	0	0.2888	1.108 e-4	0	0
	ZrO_2	0	0.3330	0	0	0
ρ	SUS304	0	8166	0	0	0
	Si_3N_4	0	2370	0	0	0
	Ti-6Al-4V	0	4420	0	0	0
	ZrO_2	0	3657	0	0	0
α	SUS304	0	12.330e-6	8.086e-4	0	0
	Si_3N_4	0	5.8723 e-6	9.095e-4	0	0
	Ti-6Al-4V	0	7.4300 e-6	7.483e-4	-3.621e-7	0
	ZrO_2	0	13.300e-6	-1.421e-3	9.549e-7	0
k	SUS304	-	15.379	-1.264e-3	2.092e-6	-7.223e-10
	Si_3N_4	-	13.723	-1.032e-3	5.466e-7	-7.876e-11
	Ti-6Al-4V	0	6.10	0	0	0
	ZrO_2	0	1.78	0	0	0

where Γ denotes a generic material property such as elastic modulus E, the Poisson's ratio ν, mass density ρ and thermal expansion coefficient α of SFGPs; furthermore subscripts m and c refer to the pure metal and ceramic plates, respectively. The expression $(x_3/h+1/2)^p$ denotes the ceramic volume fraction, where $p \geq 0$ is a namely grading index that is the volume fraction exponent. The non-linear SFGP's material can be expressed as the following [24]:

$$\rho(T) = \rho_0(\rho_{-1}T^{-1} + 1 + \rho_1 T + \rho_2 T^2 + \rho_3 T^3) \tag{2}$$

where ρ denotes material property and $T = T_0 + \Delta T(x_3)$ indicates the environmental temperature; $T_0 = 300(K)$ is room temperature; $\rho_{-1}, \rho_0, \rho_1, \rho_2$ and ρ_3 are the coefficients of temperature-dependent material properties unique to the constituent materials, and $\Delta T(x_3)$ is the temperature rise only through the thickness direction, whereas thermal conductivity k is temperature-independent. Temperature-dependent typical values for some SFGP material components such as silicon nitride and stainless steel are in Table 1 [21].

3. Elastic equations

3.1 Displacement field and strains

The displacement field based on the second-order shear deformation theory (SSDT) can be represented as [26, 31]:

$$u_1 = u + x_3\phi_1 + x_3^2\phi_2, \tag{3a}$$

$$u_2 = v + x_3\psi_1 + x_3^2\psi_2, \tag{3b}$$

$$u_3 = w \tag{3c}$$

where u_1, u_2 and u_3 denote the displacement components in the x_1, x_2 and x_3 directions, respectively; u, v and w define the displacements of a point on the mid plane $(x_1, x_2, 0)$; ϕ_1, ϕ_2, ψ_1 and ψ_2 are the rotations of a transverse normal about x_2, x_1. The displacement components $u, v, w, \phi_1, \phi_2, \psi_1, \psi_2$ and ψ_2 are functions of in-plane coordinate variables (x_1, x_2) and time t. The strain-displacement relations are given by [26, 32]:

$$\begin{Bmatrix} \varepsilon_{11} \\ \varepsilon_{22} \\ \gamma_{12} \end{Bmatrix} = \begin{Bmatrix} \varepsilon_{11}^0 \\ \varepsilon_{22}^0 \\ \gamma_{12}^0 \end{Bmatrix} + x_3 \begin{Bmatrix} \kappa_{11} \\ \kappa_{22} \\ \gamma_{12}^1 \end{Bmatrix} + x_3^2 \begin{Bmatrix} \kappa_{11}^{'} \\ \kappa_{22}^{'} \\ \gamma_{12}^2 \end{Bmatrix}, \tag{4a}$$

$$\begin{Bmatrix} \gamma_{23} \\ \gamma_{13} \end{Bmatrix} = \begin{Bmatrix} \gamma_{23}^0 \\ \gamma_{13}^0 \end{Bmatrix} + x_3 \begin{Bmatrix} \gamma_{23}^1 \\ \gamma_{13}^1 \end{Bmatrix} \tag{4b}$$

where

$$\begin{aligned} &\varepsilon_{11}^0 = \frac{\partial u}{\partial x_1}, \kappa_{11} = \frac{\partial \phi_1}{\partial x_1}, \kappa_{11}^{'} = \frac{\partial \phi_2}{\partial x_1} \\ &\varepsilon_{22}^0 = \frac{\partial v}{\partial x_2}, \kappa_{22} = \frac{\partial \psi_1}{\partial x_2}, \kappa_{22}^{'} = \frac{\partial \psi_2}{\partial x_2} \\ &\gamma_{12}^0 = (\frac{\partial u}{\partial x_2} + \frac{\partial v}{\partial x_1}), \gamma_{12}^1 = (\frac{\partial \phi_1}{\partial x_2} + \frac{\partial \psi_1}{\partial x_1}), \gamma_{12}^2 = (\frac{\partial \phi_2}{\partial x_2} + \frac{\partial \psi_2}{\partial x_1}) \\ &\gamma_{23}^0 = (\psi_1 + \frac{\partial w}{\partial x_2}), \gamma_{13}^0 = (\phi_1 + \frac{\partial w}{\partial x_1}), \gamma_{23}^1 = 2\psi_2, \gamma_{13}^1 = 2\phi_2 . \end{aligned} \tag{5}$$

3.2 Stress-strain relations

The stress-strain relation of plates is [26, 29]:

$$\begin{Bmatrix} \sigma_{11} \\ \sigma_{22} \\ \sigma_{23} \\ \sigma_{13} \\ \sigma_{12} \end{Bmatrix} = \begin{Bmatrix} q_{11} & q_{12} & 0 & 0 & 0 \\ q_{12} & q_{22} & 0 & 0 & 0 \\ 0 & 0 & q_{44} & 0 & 0 \\ 0 & 0 & 0 & q_{55} & 0 \\ 0 & 0 & 0 & 0 & q_{66} \end{Bmatrix} \begin{Bmatrix} \varepsilon_{11} \\ \varepsilon_{22} \\ \gamma_{23} \\ \gamma_{13} \\ \gamma_{12} \end{Bmatrix} \tag{6}$$

where $\gamma_{12} = 2\varepsilon_{12}$, $\gamma_{13} = 2\varepsilon_{13}$, $\gamma_{23} = 2\varepsilon_{23}$ and each q_{ij} is a function of position and temperature as follows:

$$\begin{aligned} &q_{11} = q_{22} = \frac{E(x_3, T)}{1 - \nu^2(x_3, T)} \\ &q_{12} = \nu(x_3, T) q_{11} \\ &q_{44} = q_{55} = q_{66} = \frac{E(x_3, T)}{2(1 + \nu(x_3, T))}. \end{aligned} \tag{7}$$

3.3 Equations of motion

The total strain energy of SFGP is given by $U = U_P + U_T$, where U_P and U_T are the strain energies due to mechanical and thermal effects, respectively. Considering the heating process, it can be physically observed that the plate is heated to the steady state condition after which vibration occurs in the thermally-static plate. If the temperature change ΔT is applied, the plate will undergo an initial deflection, and the corresponding initial thermal stresses occur because the plate is

constrained of the boundary supports. The strain energies U_P and U_T are given by [32-34]:

$$U_P = \frac{1}{2}\int_V [\sigma_{11}\varepsilon_{11} + \sigma_{22}\varepsilon_{22} + 2\sigma_{12}\varepsilon_{12} + 2\sigma_{23}\varepsilon_{23} + 2\sigma_{13}\varepsilon_{13}]dV = 0 \tag{8}$$

$$U_T = \frac{1}{2}\int_V [\sigma_{11}^T d_{11} + 2\sigma_{12}^T d_{12} + \sigma_{22}^T d_{22}]dV \tag{9a}$$

where $d_{ij}, (i.j = 1,2)$ is the nonlinear strain-displacement relationship [34]. By substituting d_{ij} into Eq. (9a) the following equation is obtained:

$$U_T = \frac{1}{2}\int_V \{\sigma_{11}^T[(\frac{\partial u_1}{\partial x_1})^2 + (\frac{\partial u_2}{\partial x_1})^2 + (\frac{\partial u_3}{\partial x_1})^2] + 2\sigma_{12}^T[(\frac{\partial u_1}{\partial x_1})(\frac{\partial u_1}{\partial x_2}) + (\frac{\partial u_2}{\partial x_1})(\frac{\partial u_2}{\partial x_2}) + (\frac{\partial u_3}{\partial x_1})(\frac{\partial u_3}{\partial x_2})] + \sigma_{22}^T[(\frac{\partial u_1}{\partial x_2})^2 + (\frac{\partial u_2}{\partial x_2})^2 + (\frac{\partial u_3}{\partial x_2})^2]\}dV = 0 . \tag{9b}$$

The matrix representation of the thermal conductivity tensor is diagonal because the material is assumed to be isotropic. By considering this view and the plane stress assumption, the temperature terms ${\sigma_{11}}^T$ and ${\sigma_{22}}^T$ are the only remaining terms [8, 33].

The kinetic energy of plate is given by:

$$K = \frac{1}{2}\int_V \rho(x_3,T)[\dot{u}^2 + \dot{v}^2 + \dot{w}^2]dV = 0 . \tag{10}$$

Hamilton's principle for an elastic body can be represented as:

$$\int_{t_1}^{t_2} (\delta K - \delta(U+V))dt = 0 . \tag{11}$$

The inertias are also defined as:

$$I_i = \int_{\frac{-h}{2}}^{\frac{h}{2}} \rho_0 (x_3)^i dx_3 \quad (i = 0,1,2,...,6) . \tag{12}$$

By substituting Eq. (4) into Eq. (6) and applying Eqs. (11) and (3) Navier's equations for SFGP can be obtained as follows:

$$A_{11}\frac{\partial^2 u}{\partial x_1^2} + A_{66}\frac{\partial^2 u}{\partial x_2^2} + (A_{12}+A_{66})\frac{\partial^2 v}{\partial x_1 \partial x_2} + B_{11}\frac{\partial^2 \phi_1}{\partial x_1^2} + B_{66}\frac{\partial^2 \phi_1}{\partial x_2^2} + D_{11}\frac{\partial^2 \phi_2}{\partial x_1^2} + D_{66}\frac{\partial^2 \phi_2}{\partial x_2^2} + (B_{12}+B_{66})\frac{\partial^2 \psi_1}{\partial x_1 \partial x_2} + (D_{12}+D_{66})\frac{\partial^2 \psi_2}{\partial x_1 \partial x_2} + A_{11}^T\frac{\partial^2 u}{\partial x_1^2} + B_{11}^T\frac{\partial^2 \phi_1}{\partial x_1^2} + D_{11}^T\frac{\partial^2 \phi_2}{\partial x_1^2} + A_{22}^T\frac{\partial^2 u}{\partial x_2^2} + B_{22}^T\frac{\partial^2 \phi_1}{\partial x_2^2} + D_{22}^T\frac{\partial^2 \phi_2}{\partial x_2^2} = I_0\ddot{u} + I_2\ddot{\phi}_2 + I_1\ddot{\phi}_1 \tag{13a}$$

$$A_{12}\frac{\partial^2 u}{\partial x_1 \partial x_2} + A_{66}\frac{\partial^2 u}{\partial x_1 \partial x_2} + A_{22}\frac{\partial^2 v}{\partial x_2^2} + A_{66}\frac{\partial^2 v}{\partial x_1^2} + (B_{12}+B_{66})\frac{\partial^2 \phi_1}{\partial x_1 \partial x_2} + (D_{12}+D_{66})\frac{\partial^2 \phi_2}{\partial x_1 \partial x_2} + B_{66}\frac{\partial^2 \psi_1}{\partial x_1^2} + B_{22}\frac{\partial^2 \psi_1}{\partial x_2^2} + D_{66}\frac{\partial^2 \psi_2}{\partial x_1^2} + D_{22}\frac{\partial^2 \psi_2}{\partial x_2^2} + A_{11}^T\frac{\partial^2 v}{\partial x_1^2} + B_{11}^T\frac{\partial^2 \psi_1}{\partial x_1^2} + D_{11}^T\frac{\partial^2 \psi_2}{\partial x_1^2} + A_{22}^T\frac{\partial^2 v}{\partial x_2^2} + B_{22}^T\frac{\partial^2 \psi_1}{\partial x_2^2} + D_{22}^T\frac{\partial^2 \psi_2}{\partial x_2^2} = I_0\ddot{v} + I_2\ddot{\psi}_2 + I_1\ddot{\psi}_1 \tag{13b}$$

$$A_{55}\frac{\partial \phi_1}{\partial x_1} + A_{55}\frac{\partial^2 w}{\partial x_1^2} + 2B_{55}\frac{\partial \phi_2}{\partial x_1} + A_{44}\frac{\partial \psi_1}{\partial x_2} + A_{44}\frac{\partial^2 w}{\partial x_2^2} + 2B_{44}\frac{\partial \psi_2}{\partial x_2} - A_{11}^T\frac{\partial^2 w}{\partial x_1^2} - A_{22}^T\frac{\partial^2 w}{\partial x_2^2} = I_0\ddot{w} \tag{13c}$$

$$B_{11}\frac{\partial^2 u}{\partial x_1^2} + B_{66}\frac{\partial^2 u}{\partial x_2^2} + (B_{12}+B_{66})\frac{\partial^2 v}{\partial x_1 \partial x_2} + D_{11}\frac{\partial^2 \phi_1}{\partial x_1^2} + D_{66}\frac{\partial^2 \phi_1}{\partial x_2^2} + E_{11}\frac{\partial^2 \phi_2}{\partial x_1^2} + E_{66}\frac{\partial^2 \phi_2}{\partial x_2^2} + (D_{12}+D_{66})\frac{\partial^2 \psi_1}{\partial x_1 \partial x_2} + (E_{12}+E_{66})\frac{\partial^2 \psi_2}{\partial x_1 \partial x_2} - A_{55}\left(\frac{\partial w}{\partial x_1}\right) - A_{55}\phi_1 - 2B_{55}\phi_2 - B_{11}^T\frac{\partial^2 u}{\partial x_1^2} - D_{11}^T\frac{\partial^2 \phi_1}{\partial x_1^2} - E_{11}^T\frac{\partial^2 \phi_2}{\partial x_1^2} - B_{22}^T\frac{\partial^2 u}{\partial x_2^2} - D_{22}^T\frac{\partial^2 \phi_1}{\partial x_2^2} - E_{22}^T\frac{\partial^2 \phi_2}{\partial x_2^2} = I_2\ddot{\phi}_1 + I_1\ddot{u} + I_3\ddot{\phi}_2 \tag{13d}$$

$$D_{11}\frac{\partial^2 u}{\partial x_1^2} + D_{66}\frac{\partial^2 u}{\partial x_2^2} + (D_{12}+D_{66})\frac{\partial^2 v}{\partial x_1 \partial x_2} + E_{11}\frac{\partial^2 \phi_1}{\partial x_1^2} + E_{66}\frac{\partial^2 \phi_1}{\partial x_2^2} + F_{11}\frac{\partial^2 \phi_2}{\partial x_1^2} + F_{66}\frac{\partial^2 \phi_2}{\partial x_2^2} + (E_{12}+E_{66})\frac{\partial^2 \psi_1}{\partial x_1 \partial x_2} + (F_{12}+F_{66})\frac{\partial^2 \psi_2}{\partial x_1 \partial x_2} - 2\left(B_{55}\left(\frac{\partial w}{\partial x_1}\right) + 2D_{55}\phi_2 + B_{55}\phi_1\right) - D_{11}^T\frac{\partial^2 u}{\partial x_1^2} - E_{11}^T\frac{\partial^2 \phi_1}{\partial x_1^2} - F_{11}^T\frac{\partial^2 \phi_2}{\partial x_1^2} - D_{22}^T\frac{\partial^2 u}{\partial x_2^2} - E_{22}^T\frac{\partial^2 \phi_1}{\partial x_2^2} - F_{22}^T\frac{\partial^2 \phi_2}{\partial x_2^2} = I_2\ddot{u} + I_4\ddot{\phi}_2 + I_3\ddot{\phi}_1 \tag{13e}$$

$$
\begin{aligned}
&(B_{12}+B_{66})\frac{\partial^2 u}{\partial x_1\partial x_2}+B_{22}\frac{\partial^2 v}{\partial x_2^2}+B_{66}\frac{\partial^2 v}{\partial x_1^2}-\\
&A_{44}\frac{\partial w}{\partial x_2}+(D_{12}+D_{66})\frac{\partial^2 \phi_1}{\partial x_1\partial x_2}+\\
&(E_{12}+E_{66})\frac{\partial^2 \phi_2}{\partial x_1\partial x_2}+D_{66}\frac{\partial^2 \psi_1}{\partial x_1^2}+D_{22}\frac{\partial^2 \psi_1}{\partial x_2^2}+\\
&E_{66}\frac{\partial^2 \psi_2}{\partial x_1^2}+E_{22}\frac{\partial^2 \psi_2}{\partial x_2^2}-A_{44}\psi_1-2B_{44}\psi_2-\\
&B_{11}^T\frac{\partial^2 v}{\partial x_1^2}-D_{11}^T\frac{\partial^2 \psi_1}{\partial x_1^2}-E_{11}^T\frac{\partial^2 \psi_2}{\partial x_1^2}-B_{22}^T\frac{\partial^2 v}{\partial x_2^2}-\\
&D_{22}^T\frac{\partial^2 \psi_1}{\partial x_2^2}-E_{22}^T\frac{\partial^2 \psi_2}{\partial x_2^2}=I_2\ddot{\psi}_1+I_1\ddot{v}+I_3\ddot{\psi}_2
\end{aligned}
\tag{13f}
$$

$$
\begin{aligned}
&(D_{12}+D_{66})\frac{\partial^2 u}{\partial x_1\partial x_2}+D_{66}\frac{\partial^2 v}{\partial x_1^2}+D_{22}\frac{\partial^2 v}{\partial x_2^2}-\\
&2B_{44}\frac{\partial w}{\partial x_2}+(E_{12}+E_{66})\frac{\partial^2 \phi_1}{\partial x_1\partial x_2}+\\
&(F_{12}+F_{66})\frac{\partial^2 \phi_2}{\partial x_1\partial x_2}+E_{66}\frac{\partial^2 \psi_1}{\partial x_1^2}+E_{22}\frac{\partial^2 \psi_1}{\partial x_2^2}+\\
&F_{66}\frac{\partial^2 \psi_2}{\partial x_1^2}+F_{22}\frac{\partial^2 \psi_2}{\partial x_2^2}-2B_{44}\psi_1-4D_{44}\psi_2-\\
&D_{11}^T\frac{\partial^2 v}{\partial x_1^2}-E_{11}^T\frac{\partial^2 \psi_1}{\partial x_1^2}-F_{11}^T\frac{\partial^2 \psi_2}{\partial x_1^2}-D_{22}^T\frac{\partial^2 v}{\partial x_2^2}-\\
&E_{22}^T\frac{\partial^2 \psi_1}{\partial x_2^2}-F_{22}^T\frac{\partial^2 \psi_2}{\partial x_2^2}=I_2\ddot{v}+I_4\ddot{\psi}_2+I_3\ddot{\psi}_1
\end{aligned}
\tag{13g}
$$

where $A_{ij}, B_{ij}, D_{ij}, E_{ij}$ *and* F_{ij} are the plate stiffness and $A_{ii}^T, B_{ii}^T, D_{ii}^T, E_{ii}^T$ *and* F_{ii}^T are the plate temperature stiffness.

$$
A_{ij}, B_{ij}, D_{ij}, E_{ij}, F_{ij}=\int_{\frac{-h}{2}}^{\frac{h}{2}} q_{ij}\left(1, x_3, x_3^2, x_3^3, x_3^4\right)dx_3 \tag{14a}
$$

$$
\text{for}\ \begin{cases} A_{ij}, D_{ij}, F_{ij} & (i,j=1,2,4,5,6) \\ E_{ij}, B_{ij} & (i,j=1,2,6) \end{cases} \tag{14b}
$$

$$
\begin{cases} A_{ii}^T, B_{ii}^T, D_{ii}^T, E_{ii}^T, F_{ii}^T=\displaystyle\int_{\frac{-h}{2}}^{\frac{h}{2}} \sigma_{ii}^T\left(1, x_3, x_3^2, x_3^3, x_3^4\right)dx_3 \\ (i=1,2) \end{cases} \tag{14c}
$$

$$
\begin{Bmatrix} \sigma_{11}^T \\ \sigma_{22}^T \\ \sigma_{12}^T \end{Bmatrix}=-\begin{bmatrix} q_{11} & q_{12} & 0 \\ q_{12} & q_{22} & 0 \\ 0 & 0 & q_{66} \end{bmatrix}\begin{bmatrix} 1 & 0 \\ 0 & 1 \\ 0 & 0 \end{bmatrix}\begin{bmatrix} \alpha(x_3,T) \\ \alpha(x_3,T) \end{bmatrix}\Delta T(x_3). \tag{14d}
$$

It should be noted that first-order shear deformation equations for SFGP can be obtained by considering zero values for ϕ_2 & ψ_2 in Eq. (13).

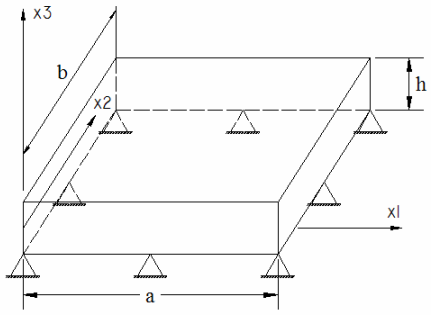

Fig. 2. Simply supported boundary condition in SFGP.

4. Boundary conditions

4.1 Mechanical boundary conditions

For an SFGP with simply support boundary conditions at the edges as shown in Fig. 2, the following relation can be written:

$$
x_1=0,a\Rightarrow \begin{cases} v(0,x_2,t)=0 \\ v(a,x_2,t)=0 \\ \psi_1(0,x_2,t)=0 \\ \psi_1(a,x_2,t)=0 \\ \psi_2(0,x_2,t)=0 \\ \psi_2(a,x_2,t)=0 \end{cases},\ \begin{cases} M_{11}(0,x_2,t)=0 \\ N_{11}(0,x_2,t)=0 \\ M_{11}(a,x_2,t)=0 \\ N_{11}(a,x_2,t)=0 \end{cases},
$$

$$
\begin{cases} w(0,x_2,t)=0 \\ w(a,x_2,t)=0 \end{cases} \tag{15a}
$$

$$
x_2=0,b\Rightarrow \begin{cases} u(x_1,0,t)=0 \\ u(x_1,b,t)=0 \\ \phi_1(x_1,0,t)=0 \\ \phi_1(x_1,b,t)=0 \\ \phi_2(x_1,0,t)=0 \\ \phi_2(x_1,b,t)=0 \end{cases},\ \begin{cases} M_{22}(x_1,0,t)=0 \\ N_{22}(x_1,0,t)=0 \\ M_{22}(x_1,b,t)=0 \\ N_{22}(x_1,b,t)=0 \end{cases},
$$

$$
\begin{cases} w(x_1,0,t)=0 \\ w(x_1,b,t)=0 \end{cases} \tag{15b}
$$

where N and M are the stress resultants.

4.2 Thermal conditions

Five cases of one-dimensional temperature distribution through the thickness (vertical, x_3) are considered, with $T=T(x_3)$.

4.2.1 Uniform temperature

In this case, a uniform temperature field of

$$
T(x_3)=T_0+\Delta T(x_3) \tag{16}
$$

is used where $\Delta T(x_3)$ denotes the temperature change and $T_0 = 300K$ is room temperature.

4.2.2 Linear temperature

Assuming temperatures T_b and T_t are imposed at the bottom and top of the plate, the temperature field under linear temperature rise along the thickness can be obtained as

$$T(x_3) = T_0 + T_b + \Delta T(\frac{x_3}{h} + \frac{1}{2}) \tag{17}$$

where $\Delta T(x_3) = T_t - T_b$ is the temperature gradient.

4.2.3 Nonlinear temperature

Consider a temperature load at the upper and lower surfaces such as

$$T = T_0 + T_t \text{ at } x_3 = \frac{h}{2} \text{ and } T = T_0 + T_b \text{ at } x_3 = -\frac{h}{2}.$$

These thermal loads can be used to solve the steady-state heat transfer Eq. (18):

$$\frac{-d}{dx_3}[k(x_3)\frac{dT}{dx}] = 0. \tag{18}$$

The temperature distribution along the thickness can be obtained:

$$T(x_3) = T_0 + T_b - (T_t - T_b)(\frac{\int_{-h/2}^{x_3} \frac{1}{k(x_3)} dx_3}{\int_{-h/2}^{h/2} \frac{1}{k(x_3)} dx_3}). \tag{19}$$

In the case of power-law SFGP, the solution of Eq. (18) also can be expressed by means of a polynomial series [35]:

$$T(x_3) = T_0 + T_b + (T_t - T_b)\Delta T(x_3) \tag{20}$$

$$\Delta T(x_3) = \frac{1}{C}\left[\begin{array}{l} \left(\frac{2x_3+h}{2h}\right) - \frac{k_{tb}}{(N+1)k_b}\left(\frac{2x_3+h}{2h}\right)^{N+1} + \\ \frac{k_{tb}^2}{(2N+1)k_b^2}\left(\frac{2x_3+h}{2h}\right)^{2N+1} - \\ -\frac{k_{tb}^3}{(3N+1)k_b^3}\left(\frac{2x_3+h}{2h}\right)^{3N+1} + \\ \frac{k_{tb}^4}{(4N+1)k_b^4}\left(\frac{2x_3+h}{2h}\right)^{4N+1} - \\ \frac{k_{tb}^5}{(5N+1)k_b^5}\left(\frac{2x_3+h}{2h}\right)^{5N+1} \end{array}\right] \tag{21}$$

$$C = \left[\begin{array}{l} 1 - \frac{k_{tb}}{(N+1)k_b} + \frac{k_{tb}^2}{(2N+1)k_b^2} - \frac{k_{tb}^3}{(3N+1)k_b^3} \\ + \frac{k_{tb}^4}{(4N+1)k_b^4} - \frac{k_{tb}^5}{(5N+1)k_b^5} \end{array}\right] \tag{22}$$

where $k_{tb} = k_t - k_b$. (23)

For an isotropic material plate, such as pure metal or ceramic plates, the temperature rise through the thickness is

$$T(x_3) = T_0 + \frac{T_t + T_b}{2} + \frac{T_t - T_b}{h} x_3. \tag{24}$$

4.2.4 Heat transfer rate by heat-flux

In this thermal condition, the heat flow from the upper surface to the lower one is assumed to be $q(W/m^2)$ and the lower surface is held at $T(x_3) = T_0 + T_b$. The heat transfer rate per unit area (heat flux) q is

$$q = -k(x_3)\frac{dT(x_3)}{dx_3}. \tag{25}$$

By solving Eq. (25) for an SFGP with the thermal conductivity varying through the thickness, the temperature rise through the thickness can be found:

$$T(x_3) = T_0 + T_b + q\int_{-h/2}^{x_3} \frac{1}{k(x_3)} dx_3. \tag{26}$$

For an isotropic material plate (pure metal or ceramic) with constant thermal conductivity, the temperature rise through the thickness is:

$$T(x_3) = T_0 + T_b + \frac{q}{k}(\frac{h}{2} + x_3). \tag{27}$$

4.2.5 Sinusoidal temperature rise

The temperature field under sinusoidal temperature rise across the thickness is assumed as [9]:

$$T(x_3) = T_0 + (T_t - T_b)\left[1 - \cos\left(\frac{\pi x_3}{2h} + \frac{\pi}{4}\right)\right] + T_b. \tag{28}$$

5. Method of solution

Based on Navier's method with simply supported boundary conditions, the displacement fields are expressed as [32]:

$$u = \sum_{n=1}^{\infty}\sum_{m=1}^{\infty} u_{mn}(t)\cos\alpha x_1 \sin\beta x_2,\ u_{mn}(t) = Ue^{-i\omega t}, \tag{29a}$$

$$v = \sum_{n=1}^{\infty}\sum_{m=1}^{\infty} v_{mn}(t)\sin\alpha x_1 \cos\beta x_2,\ v_{mn}(t) = Ve^{-i\omega t}, \tag{29b}$$

$$w=\sum_{n=1}^{\infty}\sum_{m=1}^{\infty}w_{mn}(t)\sin\alpha x_1\sin\beta x_2,\ w_{mn}(t)=We^{-i\omega t}, \quad (29c)$$

$$\phi_1=\sum_{n=1}^{\infty}\sum_{m=1}^{\infty}\phi_{1mn}(t)\cos\alpha x_1\sin\beta x_2,\ \phi_{1mn}(t)=\Phi_1e^{-i\omega t}, \quad (29d)$$

$$\phi_2=\sum_{n=1}^{\infty}\sum_{m=1}^{\infty}\phi_{2mn}(t)\cos\alpha x_1\sin\beta x_2,\ \phi_{2mn}(t)=\Phi_2e^{-i\omega t}, \quad (29e)$$

$$\psi_1=\sum_{n=1}^{\infty}\sum_{m=1}^{\infty}\psi_{1mn}(t)\sin\alpha x_1\cos\beta x_2,\ \psi_{1mn}(t)=\Psi_1e^{-i\omega t}, \quad (29f)$$

$$\psi_2=\sum_{n=1}^{\infty}\sum_{m=1}^{\infty}\psi_{2mn}(t)\sin\alpha x_1\cos\beta x_2,\ \psi_{2mn}(t)=\Psi_2e^{-i\omega t}, \quad (29g)$$

where ω is the natural frequency and

$$\alpha=\frac{m\pi}{a},\ \beta=\frac{n\pi}{b}. \quad (30)$$

Substituting the displacement fields (29) into equations of motion (13), the following frequency equation is obtained:

$$[C]\begin{Bmatrix}U\\V\\W\\\Phi_1\\\Phi_2\\\psi_1\\\psi_2\end{Bmatrix}-\omega^2[M]\begin{Bmatrix}U\\V\\W\\\Phi_1\\\Phi_2\\\psi_1\\\psi_2\end{Bmatrix}=\begin{Bmatrix}0\\0\\0\\0\\0\\0\\0\end{Bmatrix} \quad (31)$$

where stiffness matrix [C] and mass matrix [M] can be written as:

$$\begin{aligned}
C_{11}&=(A_{11}-A_{11}^T)\alpha^2+(A_{66}-A_{22}^T)\beta^2\\
C_{12}&=(A_{12}+A_{66})\alpha\beta\\
C_{13}&=0\\
C_{14}&=(B_{11}-B_{11}^T)\alpha^2+(B_{66}-B_{22}^T)\beta^2\\
C_{15}&=(D_{11}-D_{11}^T)\alpha^2+(D_{66}-D_{22}^T)\beta^2\\
C_{16}&=(B_{12}+B_{66})\alpha\beta\\
C_{17}&=(D_{12}+D_{66})\alpha\beta\\
C_{21}&=C_{12}\\
C_{22}&=(A_{66}-A_{11}^T)\alpha^2+(A_{22}-A_{22}^T)\beta^2\\
C_{23}&=0\\
C_{24}&=(B_{12}+B_{66})\alpha\beta\\
C_{25}&=(D_{12}+D_{66})\alpha\beta\\
C_{26}&=(B_{66}-B_{11}^T)\alpha^2+(B_{22}-B_{22}^T)\beta^2\\
C_{27}&=(D_{66}-D_{11}^T)\alpha^2+(D_{22}-D_{22}^T)\beta^2\\
C_{31}&=0\\
C_{32}&=0\\
C_{33}&=(A_{55}-A_{11}^T)\alpha^2+(A_{44}-A_{22}^T)\beta^2\\
C_{34}&=A_{55}\alpha\\
C_{35}&=2B_{55}\alpha\\
C_{36}&=A_{44}\beta\\
C_{37}&=2B_{44}\beta\\
C_{41}&=C_{14}\\
C_{42}&=C_{24}\\
C_{43}&=C_{34}\\
C_{44}&=(D_{11}-D_{11}^T)\alpha^2+(D_{66}-D_{22}^T)\beta^2+A_{55}\\
C_{45}&=(E_{11}-E_{11}^T)\alpha^2+(E_{66}-E_{22}^T)\beta^2+2B_{55}\\
C_{46}&=(D_{12}+D_{66})\alpha\beta\\
C_{47}&=(E_{12}+E_{66})\alpha\beta\\
C_{51}&=C_{15}\\
C_{52}&=C_{25}\\
C_{53}&=C_{35}\\
C_{54}&=C_{45}\\
C_{55}&=(F_{11}-F_{11}^T)\alpha^2+(F_{66}-F_{22}^T)\beta^2+4D_{55}\\
C_{56}&=(E_{12}+E_{66})\alpha\beta\\
C_{57}&=(F_{12}+F_{66})\alpha\beta\\
C_{61}&=C_{16}\\
C_{62}&=C_{26}\\
C_{63}&=C_{36}\\
C_{64}&=C_{46}\\
C_{65}&=C_{56}\\
C_{66}&=(D_{66}-D_{11}^T)\alpha^2+(D_{22}-D_{22}^T)\beta^2+A_{44}\\
C_{67}&=(E_{66}-E_{11}^T)\alpha^2+(E_{22}-E_{22}^T)\beta^2+2B_{44}\\
C_{71}&=C_{17}\\
C_{72}&=C_{27}\\
C_{73}&=C_{37}\\
C_{74}&=C_{47}\\
C_{75}&=C_{57}\\
C_{76}&=C_{67}\\
C_{77}&=(F_{66}-F_{11}^T)\alpha^2+(F_{22}-F_{22}^T)\beta^2+4D_{44}.
\end{aligned} \quad (32)$$

Natural frequencies and the corresponding mode shapes of SFGPs are obtained by solving the eigenvalue problem (Eq. 31).

6. Material properties in thermal conditions

The variation of Young modulus in SFGPs through the thickness in room temperature, uniform, linear, nonlinear and sinusoidal thermal conditions is presented in Figs. 3-8, respectively. Room temperature is defined at $T_0=300(K)$ for all thermal conditions. The temperature rise in uniform temperature is $T_b=T_t=600(K)$, the nonlinear thermal conditions are $T_b=0(K)$ and $T_t=600(K)$, the heat-flux thermal conditions are $T_b=0(K)$ and $q=5\times10^4(W/m^2)$ and the sinusoidal thermal conditions are $T_b=300(K)$ and $T_t=500(K)$.

It is seen from Figs. 3 and 4 that Young's modulus is simi-

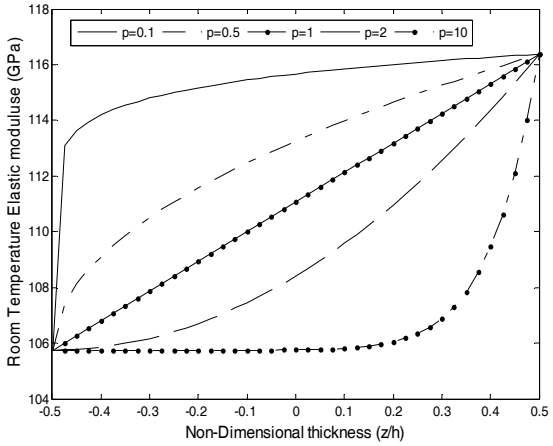

Fig. 3. Variation of Elastic modulus versus non-dimensional thickness of SFGP in room temperature field and different values of grading index (p).

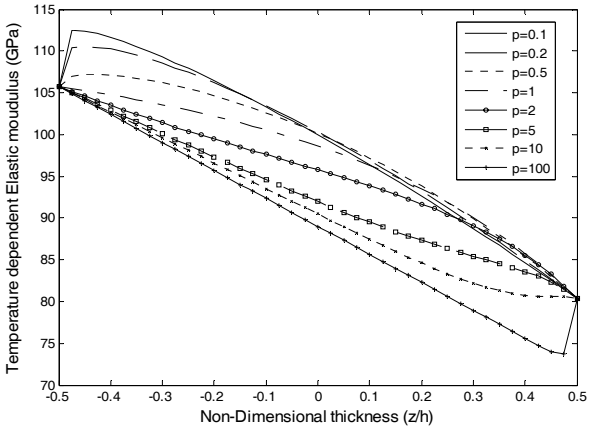

Fig. 5. Variation of Elastic modulus versus non-dimensional thickness of SFGP in nonlinear temperature field and different values of grading index (p).

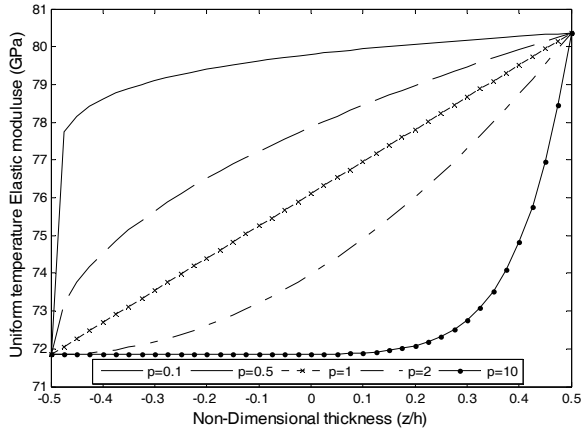

Fig. 4. Variation of Elastic modulus versus non-dimensional thickness of SFGP in linear temperature field and different values of grading index (p).

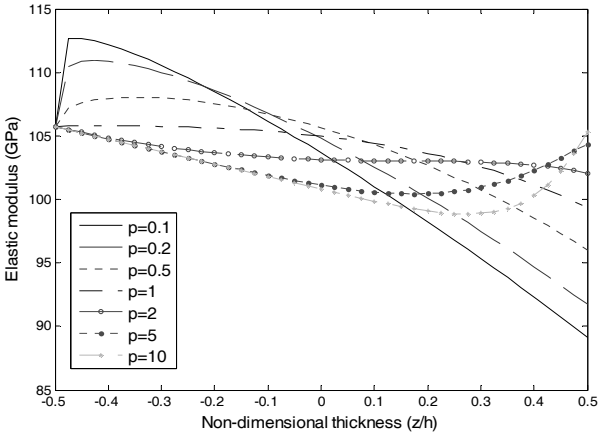

Fig. 6. Variation of Elastic modulus versus non-dimensional thickness of SFGP in heat flux temperature field and different values of grading index (p).

lar for conditions with room temperature and uniform temperature, but the graphs move to smaller values with the uniform temperature rise. It is clear that Young's modulus decreases with the increase of the grading index. Figs. 3-8 show that the behavior of Young's modulus in nonlinear, heat flux and sinusoidal thermal loads is completely different from that in room and uniform temperature cases.

In nonlinear and sinusoidal thermal conditions (Figs. 5 and 7), the value of Young's modulus increases close to the lower surface, then decreases when $p<1$, and the modulus decreases when $1 \le p < 10$. However, Young's modulus decreases then increases close to upper surface for the large value of grading index ($p>10$) in nonlinear and sinusoidal thermal conditions.

The nonlinear thermal conditions are $T_b = 0(K)$ and $T_t = 600(K)$, which means that the temperature at the upper surface (ceramic-rich) is higher than the temperature of the lower surface (metal-rich). This may result from the fact that the elastic modulus decreases in the ceramic-rich surface. It is clearly extracted by considering Eq. 1 so that if $x_3/h = 0.5$ then the elastic modulus can be expressed as $E = E(x_3, T) = E_c(T)$. It is shown that when $x_3/h = 0.5$, the elastic modulus is equal to the elastic modulus of ceramic-rich material at 600(K), which is less than the elastic modulus of metal-rich at 0(K).

In heat-flux thermal condition (Fig. 6) the elastic modulus at the upper surface increases with the increase of the grading index. These phenomena can be explained in that as the value of the grading index increases (see Eq. (1)), the volume fraction of ceramic is increased and the heat flow is more restricted. Comparison of Young's modulus has been made for uniform, linear, nonlinear, heat-flux and sinusoidal thermal conditions in Fig. 8. It can be seen that Young's modulus increases close to the lower surface for all thermal loads and then decreases through the thickness except in the uniform thermal condition.

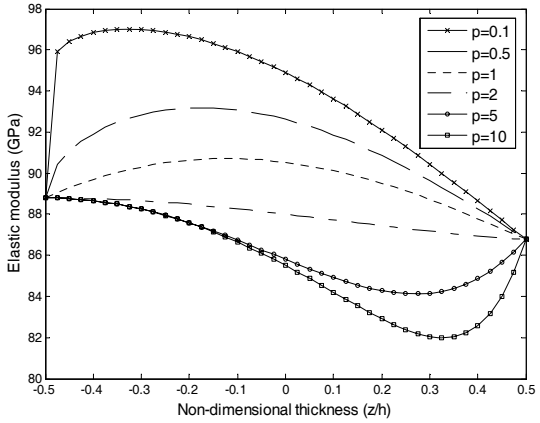

Fig. 7. Variation of Elastic modulus versus non-dimensional thickness of SFGP in sinusoidal temperature field and different values of grading index (p).

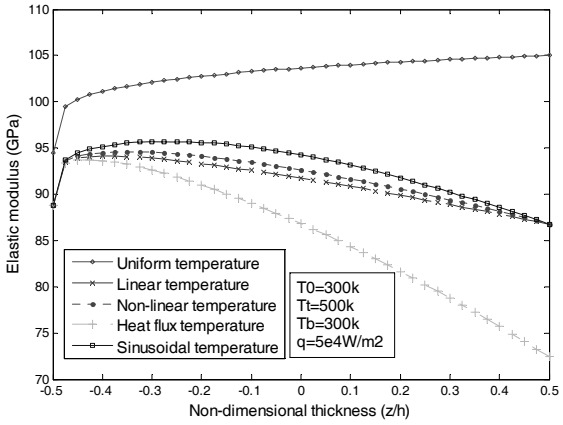

Fig. 8. Variation of Elastic modulus versus non-dimensional thickness of SFGP in uniform, linear, nonlinear, heat flux and sinusoidal temperature field and different values of grading index (p).

7. Validation and numerical results

7.1 Validation

The results for temperature-dependent SFGP obtained by applying SSDT in this study are compared by adapting the higher-order shear deformation theory results [19]. The following non-dimensional fundamental frequencies in Table 2 are obtained by considering a combination of ZrO_2/Ti–6Al–4V where the upper surface is ceramic-rich and the lower surface is metal-rich [19]. In accordance with [19], the dimension-less natural frequency parameter is $\bar{\omega} = \omega(a^2/h)[\rho_b(1-\nu^2)/E_b]^{1/2}$ where E_b and ρ_b are at T_0 = 300(K). Validation has been done by considering the values of thickness, side, Poisson's ratio, density and thermal conductivity in the ceramic and metal as:

$$h = 0.025m\ ,\ a = 0.2m\ ,\ \nu = 0.3\ ,\ \rho_C = 3000\,kg/m^3$$
$$\kappa_C = 1.80\,W/mK\ ,\ \rho_m = 4429\,kg/m^3\ ,\ \kappa_m = 7.82\,W/mK\ .$$

Table 2. Non-dimensional natural frequency parameter (ZrO_2/Ti-6Al-4V) SFGP for simply supported in thermal environments.

Mode (1,1) Natural frequency of SFGP (ZrO_2 and Ti-6Al-4V)		$T_b = 300k$				
		$T_t = 300k$	$T_t = 400k$		$T_t = 600k$	
			Temperature-dependent	Temperature-independent	Temperature-dependent	Temperature-independent
ZrO_2	Present	8.333	7.614	7.892	5.469	6.924
	Ref. [19]	8.273	7.868	8.122	6.685	7.686
p=0.5	Present	7.156	6.651	6.844	5.255	6.175
	Ref. [19]	7.139	6.876	7.154	6.123	6.776
p=1	Present	6.700	6.281	6.446	5.167	5.904
	Ref. [19]	6.657	6.437	6.592	5.819	6.362
p=2	Present	6.333	5.992	6.132	5.139	5.711
	Ref. [19]	6.286	6.101	6.238	5.612	6.056
Ti-6Al-4V	Present	5.439	5.103	5.333	4.836	5.115
	Ref. [19]	5.400	5.322	5.389	5.118	5.284

The same value of Poisson's ratio υ is considered for the ceramic and metal. Young's modulus and thermal expansion coefficient of these materials are assumed to be temperature-dependent and listed in Ref. [19]. Table 2 shows the natural frequencies obtained from the present study using SSDT and Huang [19].

There is a considerable agreement between the presented results and those from Ref. [19], especially for thick plates. The main reason which can explain the difference between presented results in Table 2 and Ref. [19] is the difference between SSDT and HSDT. The results from the present study by SSDT are greater than those from the higher-order shear deformation theory (HSDT, Ref. [19]). This phenomenon can be described as that the transverse shear and rotary inertia have more effect on thick plate. Moreover, the transverse shear strains in HSDT are assumed to be parabolically distributed across the plate thickness. Due to greater accuracy HSDTs use higher-order polynomials in the expansion of the displacement components through the thickness of the plate. The HSDTs introduce additional unknowns that are often difficult to interpret in physical terms. In principle, one may expand the displacement field of a plate in terms of the thickness variable up to any desired degree. However, due to the algebraic complexity and computational effort involved with HSDTs in return for a marginal gain in accuracy, theories higher than second order have not been attempted in this research. For the thick plates considered in this case, there is less difference between the result predicted by SSDT and HSDT; the SSDT slightly over-predicts the frequencies.

The natural frequencies can be decreased by increasing $\Delta T(x_3)$ because the modulus of elasticity decreases with rising temperatures. It can be noted that the natural frequency in temperature-dependent SFGPs is greater than those in tem-

Table 3. Non-dimensional frequency parameter (ZrO_2/Ti-6Al-4V) SFGP for simply supported in thermal environments.

Mode numbers of SFGP (ZrO_2& Ti-6Al-4V)		$T_b = 300k$				
		$T_t = 300k$	$T_t = 400k$		$T_t = 600k$	
			Temperature-dependent	Temperature-independent	Temperature-dependent	Temperature-independent
ZrO_2	(1,1)	8.333	7.614	7.892	5.469	6.924
	(1,2)	19.613	18.585	19.151	16.092	18.191
	(2,2)	29.785	28.471	29.300	25.518	28.305
	(1,3)	36.084	34.588	35.584	31.331	34.562
	(2,3)	44.942	43.192	44.420	39.506	43.359
p=0.5	(1,1)	7.156	6.651	6.844	5.255	6.175
	(1,2)	16.852	16.126	16.527	14.431	15.859
	(2,2)	25.604	24.677	25.263	22.647	24.567
	(1,3)	31.036	29.981	30.684	27.734	29.970
	(2,3)	38.670	37.439	38.304	34.887	37.562
p=1	(1,1)	6.700	6.281	6.446	5.167	5.904
	(1,2)	15.774	15.161	15.507	13.765	14.960
	(2,2)	23.959	23.172	23.679	21.482	23.109
	(1,3)	29.040	28.143	28.752	26.264	28.167
	(2,3)	36.176	35.128	35.876	32.985	35.268
p=2	(1,1)	6.333	5.992	6.132	5.139	5.711
	(1,2)	14.896	14.383	14.684	13.260	14.253
	(2,2)	22.608	21.942	22.386	20.557	21.935
	(1,3)	27.392	26.630	27.163	25.077	26.700
	(2,3)	34.106	33.211	33.867	31.425	33.384
Ti-6Al-4V	(1,1)	5.439	5.103	5.333	4.836	5.115
	(1,2)	12.801	12.130	12.689	11.655	12.463
	(2,2)	19.440	18.467	19.323	17.802	19.085
	(1,3)	23.551	22.390	23.430	21.604	23.185
	(2,3)	29.333	27.907	29.206	26.954	28.951

Table 4. Non-dimensional natural frequency parameter (Si_3N_4/ SUS304) SFGP for simply supported in thermal environments.

Mode numbers of SFGP (Si_3N_4& SUS304)		$T_b = 300k$				
		$T_t = 300k$	$T_t = 400k$		$T_t = 600k$	
			Temperature-dependent	Temperature-independent	Temperature-dependent	Temperature-independent
Si_3N_4	(1,1)	12.506	12.175	12.248	11.461	11.716
	(1,2)	29.464	29.030	29.192	28.138	28.641
	(2,2)	44.782	44.253	44.496	43.190	43.919
	(1,3)	54.277	53.687	53.982	52.514	53.388
	(2,3)	67.641	66.967	67.334	65.640	66.715
p=0.5	(1,1)	8.652	8.361	8.405	7.708	7.887
	(1,2)	20.355	20.001	20.095	19.233	19.565
	(2,2)	30.902	30.491	30.629	29.605	30.076
	(1,3)	37.439	36.991	37.157	36.029	36.588
	(2,3)	46.621	46.122	46.328	45.055	45.736
p=1	(1,1)	7.584	7.306	7.342	6.674	6.834
	(1,2)	17.841	17.512	17.587	16.781	17.068
	(2,2)	27.082	26.707	26.816	25.871	26.275
	(1,3)	32.813	32.407	32.538	31.504	31.981
	(2,3)	40.858	40.411	40.572	39.413	39.993
p=2	(1,1)	6.811	6.545	6.575	5.929	6.077
	(1,2)	16.017	15.708	15.769	15.002	15.262
	(2,2)	24.307	23.958	24.047	23.154	23.517
	(1,3)	29.446	29.071	29.177	28.204	28.632
	(2,3)	36.657	36.247	36.376	35.290	35.809
SUS304	(1,1)	5.410	5.161	5.178	4.526	4.682
	(1,2)	12.745	12.471	12.503	11.729	12.004
	(2,2)	19.372	19.073	19.117	18.214	18.599
	(1,3)	23.479	23.164	23.217	22.229	22.684
	(2,3)	29.260	28.923	28.987	27.881	28.433

perature-independent SFGPs. As expected, natural frequencies in pure ceramic are greater than those in pure metal and results for SFGPs are in between.

7.2 Numerical results

Tables 3 and 4 show the natural frequencies in ZrO_2/Ti–6Al–4V and Si_3N_4/SUS304 for different thermal loads, respectively. The non-dimensional natural frequency parameter is defined as $\bar{\omega} = \omega(a^2/h)[\rho_b(1-\nu^2)/E_b]^{1/2}$ where E_b and ρ_b are at T_0 = 300 (K) [19]. The effect of volume fraction index p on the frequencies can be seen by considering the same value of thermal load and shape mode. The result for SFGPs is in between those for pure material plates, because Young's modulus decreases from pure ceramic to pure metal. The frequencies are decreased by increasing the temperature difference between top and bottom surfaces for the same value of grading index and shape mode that represent the effects of thermal loads. The comparison between temperature-dependent and independent SFGPs in Tables 3 and 4 reveals the smaller frequencies in temperature-dependent SFGPs, which demonstrates the accuracy and effectiveness of temperature-dependent material properties.

The behavior of natural frequencies for Si_3N_4/SUS304 in Table 4 is similar to those for ZrO_2/Ti–6Al–4V in Table 3. The value of natural frequency for Si_3N_4/SUS304 is greater than that for ZrO_2/Ti–6Al–4V due to higher modulus of elasticity of Si_3N_4 compared with ZrO_2. It is worth mentioning that the difference of natural frequency for the same temperature and shape mode is decreased with the increase of grading index. This phenomenon is because the stiffnesses for Ti–6Al–4V and SUS304 are close to each other.

Table 5 shows the natural frequencies in Si_3N_4/SUS304 for large value of volume fraction index (p) and different values of thermal loads. As described before, the non-dimensional natural frequency parameter is defined as $\bar{\omega} = \omega(a^2/h)$

Table 5. Non-dimensional natural frequency of temperature dependent (Si_3N_4& SUS304) SFGP for different volume fraction index (p) in thermal environments.

Thermal loads $T_0 = 0k$, $b = a = 0.2$, $h = 0.025$		$T_b = 300k$ $T_b = 300k$	$T_b = 300k$ $T_t = 400k$	$T_b = 300k$ $T_b = 600k$
Non-dimensional natural frequency of temperature dependent SFGP (Si_3N_4 & SUS304) for different volume fraction index (p) and thermal load, Mode (1,1)	Full ceramic	12.506	12.175	11.461
	$p = 5$	6.200	5.936	5.328
	$p = 10$	5.907	5.645	5.031
	$p = 20$	5.711	5.450	4.825
	$p = 40$	5.591	5.329	4.694
	$p = 60$	5.546	5.284	4.645
	$p = 80$	5.523	5.260	4.619
	$p = 100$	5.508	5.246	4.603
	Full metal	5.410	5.161	4.526

$[\rho_b(1-\nu^2)/E_b]^{1/2}$ where E_b and ρ_b are at T_0 = 300 (K) [19]. The frequencies are decreased by increasing the volume fraction index (p) and by decreasing the temperature difference between the top and bottom surfaces for the same value of grading index and shape mode that represent the effects of thermal loads. This is expected, because a larger volume fraction index means that a plate has a smaller ceramic component and that its stiffness is thus reduced. A uniform frequency distribution for values of (p) is virtually predictable, but the trend of variation is not linear as (p) increases.

The following numerical results are obtained by considering the combination of titanium alloy (Ti–6Al–4V) as the lower surface and zirconium oxide (ZrO2) as the upper surface in SFGPs according to Table 1. The geometry of square SFGPs is as follows:

$a/h = 10$ (side-to-thickness ratio),
$a = 0.2m$ (side of the square).

The variation of temperature distribution through the thickness of SFGPs is shown in Figs. 9 and 10 by applying nonlinear and heat-flux thermal conditions, respectively. The upper surface is held at T_t = 1000 (K), and the lower surface is held at T_b = 300 (K) in Fig. 10.

For pure-material plates, temperature distributions are the same regardless of the material type. The temperature at any internal point through the thickness of a plate made of pure material ($p = 0$ and $p \to \infty$) is always higher than that corresponding to SFGP. In contrast to the linear temperature distribution in a pure plate, the variation of temperature through the thickness in SFGPs is non-linear.

Fig. 10 shows temperature distributions through the thickness of SFGPs subjected to heat-flux thermal condition. It is assumed that the lower surface is held at T_b = 0 (K) (T_0 = 300 (K)) and the heat-flow from the upper surface to the lower is q = 5 x 10^4 W/m^2.

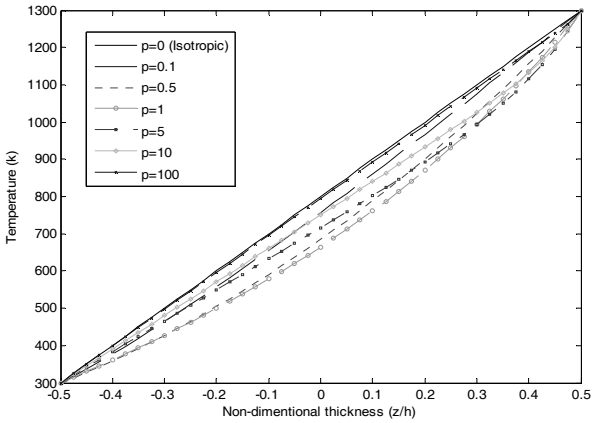

Fig. 9. Variation of nonlinear temperature field versus non-dimensional thickness of SFGP for different values of grading index (p) .

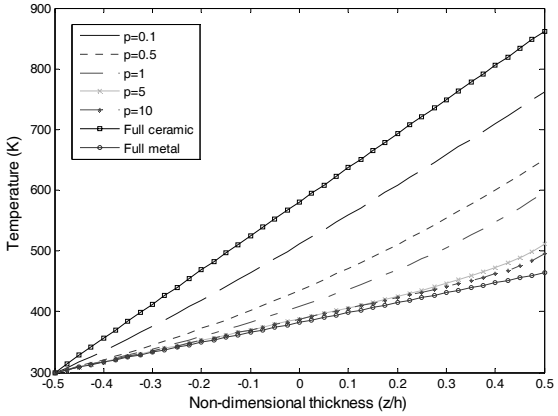

Fig. 10. Variation of heat flux temperature field versus non-dimensional thickness of SFGP for different values of grading index (p) .

The temperature distributions are at a maximum for pure ceramic and a minimum for pure metal with different SFGPs falling in between. In contrast to the result for nonlinear thermal loads, the trade of temperature variation is linear in SFGPs.

The temperature distributions of SFGPs under linear, nonlinear, sinusoidal and heat flux thermal conditions along the thickness direction are shown in Fig. 11. It is considered that the upper and lower surfaces are held at T_t = 500 (K) and T_b = 300 (K) and room temperature is T_0 = 300 (K). Four cases, namely linear, non-linear, sinusoidal and heat flux, are considered. For heat-flux, the source from upper to lower surface is applied as q = 5 x 10^4 (W/m^2). It is absorbed that the variation of temperature through the thickness is the lowest for sinusoidal temperature load. Linear thermal load creates the greater temperature in comparison with non-linear thermal load. As expected, the variation of temperature in existence of heat flux is larger than the other results. It is also plotted that the curve of linear temperature condition is close to nonlinear temperature condition.

The following dimensionless frequencies are presented by

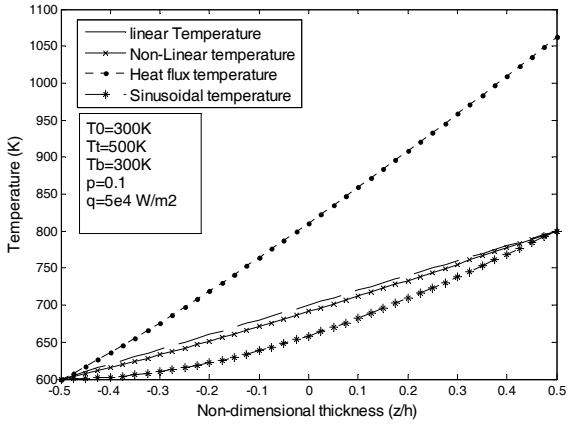

Fig. 11. Variation of linear, nonlinear, heat flux and sinusoidal temperature field versus non-dimensional thickness of SFGP for different values of grading index (p) .

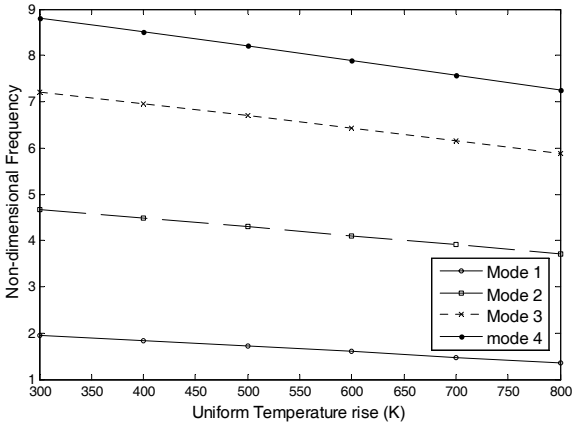

Fig. 12. First four Non-dimensional frequency parameters versus uniform temperature field for simply supported (ZrO_2/Ti-6Al-4V) SFGP when $a/h=10$ and $a=0.2,\ p=1$.

using non-dimensional parameters [33]:

$$\bar{\omega}=\frac{\omega b^2}{\pi^2}\sqrt{\frac{I_0}{D_0}}$$

where

$$I_0=\rho h \quad \text{and} \quad D_0=Eh^3/12(1-\upsilon^2)\,.$$

It is noted that ρ, ν and E are chosen to be the values of Ti-6Al-4V evaluated at the room temperature.

The room temperature is considered $T_0=300\,(K)$ for all thermal conditions. The temperature rise is $T_b=0\,(K)$ & $T_t=500\,(K)$ in uniform, linear, nonlinear and sinusoidal thermal conditions. The thermal condition in heat-flux case is $T_b=500\,(K)$ and $q=1\times10^3(W/m^2)$ at the bottom surface toward the upper surface.

Figs. 12-16 show the first four frequencies versus uniform, linear, nonlinear, heat flux and sinusoidal temperature fields in simply supported SFGP. The combination of ZrO_2/Ti-6Al-4V as shown in Table 1 is considered with material and geometric parameters of $p=1,\ a=0.2$ and $a/h=10$.

As expected, the decrease of Young's modulus with rising temperatures leads to the frequencies decreasing with increasing temperature. The decreasing slope of frequencies in higher modes is greater than those in smaller modes. The difference between two consequence higher modes is smaller than that in two consequence lower modes at the same temperature. It is evident that the temperature rise effect in uniform temperature condition is more significant than other thermal conditions. It can be explained in that the decreasing slope frequency in linear, nonlinear and sinusoidal thermal loads is almost the same while decreasing slope frequency is greater than other thermal conditions in uniform thermal load. It is displayed that the decreasing slope frequency is very small in heat-flux thermal condition.

Figs. 17 and 18 investigate the effect of side-to-side ratio versus nonlinear and sinusoidal thermal loads of simply supported SFGP. The combination of ZrO_2/Ti-6Al-4V as shown in Table 1 is considered while the material and geometric parameters are $p=2,\ a=0.2$ and $a/h=10$. It can be dis-

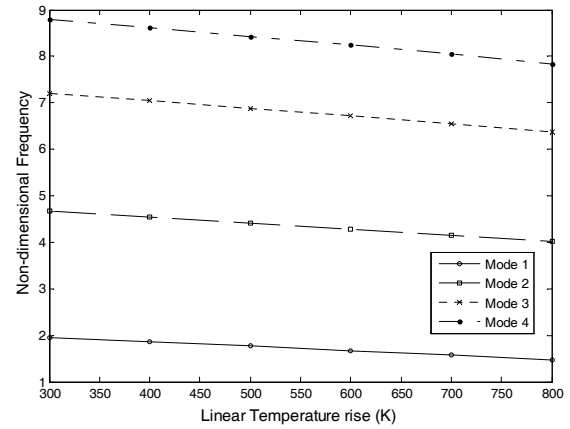

Fig. 13. First four Non-dimensional frequency parameters versus linear temperature field for simply supported (ZrO_2/Ti-6Al-4V) SFGP when $a/h=10$ and $a=0.2,\ p=1$.

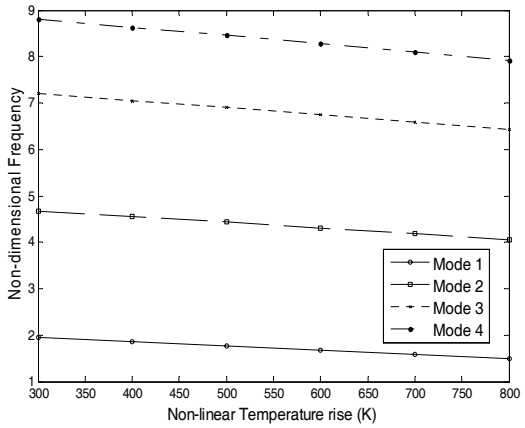

Fig. 14. First four Non-dimensional frequency parameters versus nonlinear temperature field for simply supported (ZrO_2/Ti-6Al-4V) SFGP when $a/h=10$ and $a=0.2,\ p=1$.

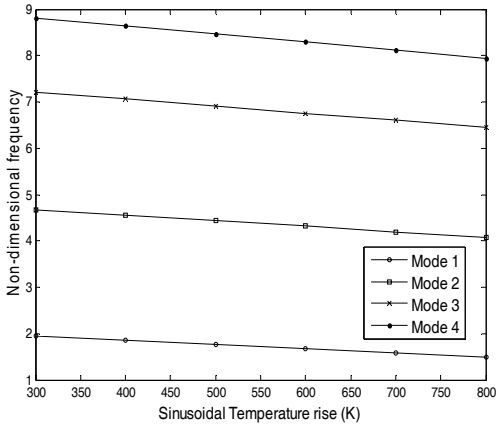

Fig. 15. First four Non-dimensional frequency parameters versus sinusoidal temperature field for simply supported (ZrO_2/Ti-6Al-4V) SFGP when $a/h=10$ and $a=0.2,\ p=1$.

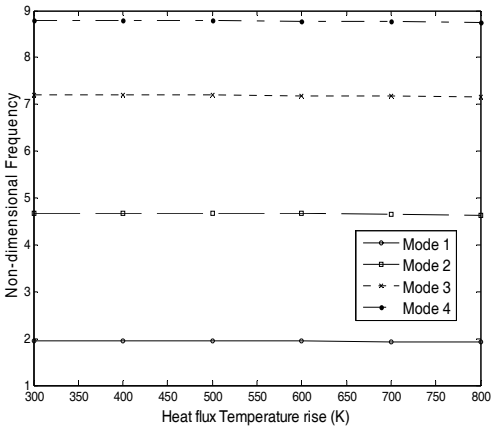

Fig. 16. First four Non-dimensional frequency parameters versus heat flux temperature field for simply supported (ZrO_2/Ti-6Al-4V) SFGP when $a/h=10$ and $a=0.2,\ p=1$.

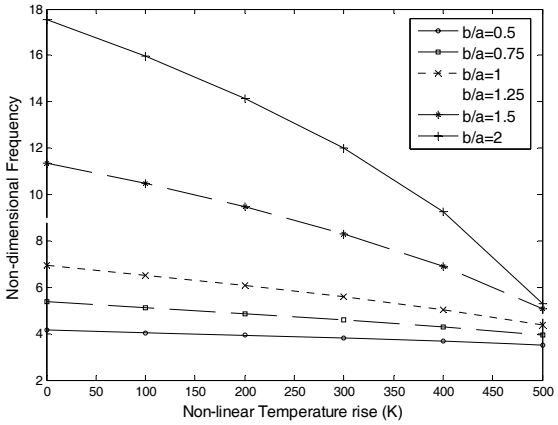

Fig. 17. Non-dimensional frequency parameters versus nonlinear temperature field for different values of side-to-side ratio (b/a) and simply supported (ZrO_2/Ti-6Al-4V) SFGP when $a/h=10$ and $a=0.2,\ p=2$.

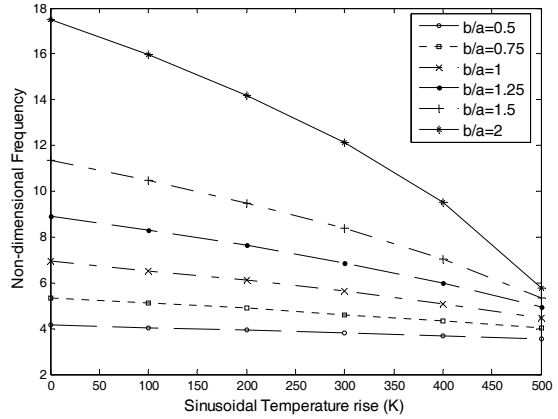

Fig. 18. Non-dimensional frequency parameters versus sinusoidal temperature field for different values of side-to-side ratio (b/a) and simply supported (ZrO_2/Ti-6Al-4V) SFGP when $a/h=10$ and $a=0.2,\ p=2$.

played that in Figs. 17 and 18, due to gradation of stiffness, the frequencies increase with the increase of the b/a while $b/a \le 2$. As expected, the frequency decreases as ΔT increases for nonlinear and sinusoidal temperature fields because Young's modulus decreases with rising temperatures. It is also seen that the decreasing slope frequency for $b/a=2$ is greater than other side-to-side ratio while side-to-thickness ratio is equal to ten $(a/h=10)$ in SFGP.

8. Conclusion

Temperature-dependent free vibration of solar functionally graded plates subjected to uniform, linear, nonlinear, heat-flux and sinusoidal temperature fields are investigated by using an analytical approach (Navier's Method) for simply supported SFGP. The formulations are based on the second-order shear deformation theory (SSDT) to account for transverse shear effects through the thickness. Material properties of SFGPs are assumed to be temperature-dependent and vary along the thickness by a power-law distribution in terms of volume fractions of constituents. The results are validated by comparing them with the results of other researchers, with good agreement. Some general conclusions of this study can be summarized as follows:

Free vibration is at the maximum for pure ceramic, the minimum for pure metal, and degrades gradually as the volume fraction index p increases.

The frequency decreases as temperature change (ΔT) increases in all types of temperature fields.

The uniform and heat flux temperature fields affect the frequencies more significantly than the linear, nonlinear and sinusoidal temperature fields.

The value of temperature increases with decreasing grading index (p).

The frequencies of SFGPs with higher grading index are more sensitive to the temperature rise than those for other grading index.

The frequencies increase with the increase of the side-to-

side ratio (b/a) while $b/a < 2$.

From the numerical results presented in this study it appears that the SSDT results are greater than those from higher order shear deformation theory (HSDT). It is suggested that the gradation of the constitutive components, geometry and temperature rise are significant parameters in the frequency of solar functionally graded plates.

Acknowledgment

This work supported by Universiti Putra Malaysia for providing the research grant (FRGS 07-10-07-398SFR 5523398).

References

[1] Y. Howell and J. Bereny, *Engineer's guide to solar energy*, Solar Energy Information Services (1979).

[2] M. Bayat, M. Saleem, B. Sahari, A. Hamouda and E. Mahdi, Analysis of functionally graded rotating disks with variable thickness, *Mechanics Research Communications*, 35 (5) (2008) 283-309.

[3] M. Bayat, M. Saleem, B. Sahari, A. Hamouda and E. Mahdi, Mechanical and thermal stresses in a functionally graded rotating disk with variable thickness due to radially symmetry loads, *International Journal of Pressure Vessels and Piping*, 86 (6) (2009) 357-372.

[4] R. Naj, M. Sabzikar Boroujerdy and M. Eslami, Thermal and mechanical instability of functionally graded truncated conical shells, *Thin-Walled Structures*, 46 (1) (2008) 65-78.

[5] J. Reddy and N. Phan, Stability and vibration of isotropic, orthotropic and laminated plates according to a higher-order shear deformation theory, *Journal of Sound and Vibration*, 98 (2) (1985) 157-170.

[6] S. Xiang and K. Wang, Free vibration analysis of symmetric laminated composite plates by trigonometric shear deformation theory and inverse multiquadric RBF, *Thin-Walled Structures*, 47 (3) (2009) 304-310.

[7] R. Batra, Higher-order shear and normal deformable theory for functionally graded incompressible linear elastic plates, *Thin-Walled Structures*, 45 (12) (2007) 974-982.

[8] G. Praveen and J. Reddy, Nonlinear transient thermoelastic analysis of functionally graded ceramic-metal plates, *International Journal of Solids and Structures*, 35 (1998) 4457-4476.

[9] B. Mokhtar, T. Abedlouahed, A. El Abbas and M. Abdelkader, Buckling Analysis of Functionally Graded Plates with Simply Supported Edges, *Leonardo Journal of Sciences*, 8 (2009) 21-32.

[10] K. Shukla, Nonlinear static and dynamic analysis of functionally graded plates *Int. J. of Appl. Mech. and Eng.*, 11 (3) (2006) 679-698.

[11] H. Ibrahim, H. Yoo, M. Tawfik and K. Lee, Thermo-acoustic random response of temperature-dependent functionally graded material panels, *Computational Mechanics* 1-10.

[12] J. Park and J. Kim, Thermal postbuckling and vibration analyses of functionally graded plates, *Journal of Sound and Vibration*, 289 (1-2) (2006) 77-93.

[13] X. Zhao, Y. Lee and K. Liew, Free vibration analysis of functionally graded plates using the element-free kp-Ritz method, *Journal of Sound and Vibration*, 319 (3-5) (2009) 918-939.

[14] A. Ferreira, R. Batra, C. Roque, L. Qian and R. Jorge, Natural frequencies of functionally graded plates by a meshless method, *Composite Structures*, 75 (1-4) (2006) 593-600.

[15] M. Bayat, M. Saleem, B. Sahari, A. Hamouda and E. Mahdi, Thermo elastic analysis of a functionally graded rotating disk with small and large deflections, *Thin-Walled Structures*, 45 (7-8) (2007) 677-691.

[16] M. Bayat, B. Sahari, M. Saleem, A. Ali and S. Wong, Thermoelastic solution of a functionally graded variable thickness rotating disk with bending based on the first-order shear deformation theory, *Thin-Walled Structures*, 47 (5) (2009) 568-582.

[17] R. Batra and J. Jin, Natural frequencies of a functionally graded anisotropic rectangular plate, *Journal of Sound and Vibration*, 282 (1-2) (2005) 509-516.

[18] C. Dong, Three-dimensional free vibration analysis of functionally graded annular plates using the Chebyshev-Ritz method, *Materials & Design*, 29 (8) (2008) 1518-1525.

[19] X. Huang and H. Shen, Nonlinear vibration and dynamic response of functionally graded plates in thermal environments, *International Journal of Solids and Structures*, 41 (9-10) (2004) 2403-2427.

[20] H. Matsunaga, Thermal buckling of functionally graded plates according to a 2D higher-order deformation theory, *Composite Structures*, 90 (1) (2009) 76-86.

[21] Y. Kim, Temperature dependent vibration analysis of functionally graded rectangular plates, *Journal of Sound and Vibration*, 284 (3-5) (2005) 531-549.

[22] N. Sundararajan, T. Prakash and M. Ganapathi, Nonlinear free flexural vibrations of functionally graded rectangular and skew plates under thermal environments, *Finite Elements in Analysis and Design*, 42 (2) (2005) 152-168.

[23] C. Chen, T. Chen and R. Chien, Nonlinear vibration of initially stressed functionally graded plates, *Thin-Walled Structures*, 44 (8) (2006) 844-851.

[24] J. Yang and H. Shen, Vibration characteristics and transient response of shear-deformable functionally graded plates in thermal environments, *Journal of Sound and Vibration*, 255 (3) (2002) 579-602.

[25] J. Yang and H. Shen, Free vibration and parametric resonance of shear deformable functionally graded cylindrical panels, *Journal of Sound and Vibration*, 261 (5) (2003) 871-893.

[26] A. Khdeir and J. Reddy, Free vibrations of laminated composite plates using second-order shear deformation theory, *Computers & Structures*, 71 (6) (1999) 617-626.

[27] A. R. Saidi and S. Sahraee, Axisymmetric solutions of functionally graded circular and annular plates using second-order shear deformation plate theory, *Proceedings of 8th Bi-*

ennial ASME Conference on Engineering Systems Design and Analysis, ESDA2006 (2006)

[28] A. Shahrjerdi, M. Bayat, F. Mustapha, S. Sapuan and R. Zahari, Free Vibration Analysis of Functionally Graded Quadrangle Plates Using Second Order Shear Deformation Theory, *Australian Journal of Basic and Applied Sciences*, 4 (5) (2010) 893-905.

[29] A. Shahrjerdi, M. Bayat, F. Mustapha, S. Sapuan and R. Zahari, Second-Order Shear Deformation Theory to Analyze Stress Distribution for Solar Functionally Graded Plates, *Mechanics Based Design of Structures and Machines*, 38 (3) (2010) 348-361.

[30] A. Bahtui and M. Eslami, Coupled thermoelasticity of functionally graded cylindrical shells, *Mechanics research communications*, 34 (1) (2007) 1-18.

[31] A. Shahrjerdi, M. Bayat, F. Mustapha, S. Sapuan and R. Zahari, Stress Analysis a Functionally Graded Quadrangle Plate Using Second Order Shear Deformation Theory, *International Review of Mechanical Engineering*, 4 (1) (2010) 92-105.

[32] J. N. Reddy, Theory and analysis of elastic plates and shells, Taylor Print on DEMA (2006).

[33] Q. Li, V. Iu, and K. Kou, Three-dimensional vibration analysis of functionally graded material plates in thermal environment, *Journal of Sound and Vibration*, 324 (3-5) (2009) 733-750.

[34] J. N. Reddy, *Mechanics of laminated composite plates and shells*, CRC press (2004).

[35] R. Javaheri and M. Eslami, Thermal buckling of functionally graded plates based on higher order theory, *Journal of Thermal Stresses*, 25 (7) (2002) 603-625.

Ali Shahrjerdi is a member of the Mechanical Engineering department in Malayer University, Iran. He received a Ph.D in Mechanical Engineering from the University Putra Malaysia. His research interests include finite element analysis, numerical methods, aircraft design, composites and functionally graded materials.